A Discrete Scintillation Camera Module Using Silicon Photodiode Readout of CsI(Tl) Crystals for Breast Cancer Imaging[1]

G.J. Gruber, W.W. Moses, *Senior Member, IEEE*, S.E. Derenzo, *Senior Member, IEEE*, N.W. Wang, E. Beuville, and M.H. Ho

Lawrence Berkeley National Laboratory, University of California, Berkeley, CA 94720

Abstract

We characterize a 2x4 element imaging array consisting of 1x3x5 mm³ CsI(Tl) scintillator crystals individually read out by 3x3 cm² PIN silicon photodiodes. The array is a prototype for larger modules (16x16 element) for use in single photon breast cancer imaging. The photodiode output signals are amplified with a 16 channel custom IC (<3 cm on a side), after which a "Winner Take All" (WTA) custom IC (<3 cm on a side) identifies the crystal of interaction based on relative signal amplitudes. The compact nature of these readout electronics will simplify the construction of larger imaging arrays. The photodiodes were developed for low leakage current (~50 pA) and yield a total electronic noise of 390 e- full width at half maximum (FWHM) at a shaping time of 8 μs, with signal levels of 6600 e- for the 140 keV emissions of ^{99m}Tc. Array pixels demonstrate an average room temperature energy resolution of 10.7±0.6% FWHM for the 140 keV gamma rays. We observe an intrinsic spatial resolution of 3.3 mm FWHM for a 2.5 mm diameter ^{57}Co beam on the face of the crystal array, and a system resolution of 5.0 mm FWHM for a 2 mm diameter uncollimated ^{99m}Tc source viewed through a high resolution hexagonal hole collimator (1.5 mm hole diameter, 33 mm length, #300 events/mCi/sec) at an imaging distance of 5 cm.

I. Introduction

Recent research has demonstrated that scintimammography imaging with minor-avid tracers (most commonly ^{99m}Tc-Sestamibi) and standard scintillation cameras can accurately diagnose primary breast cancer, demonstrating sensitivities of 80–94% and specificities of 73–93% [1–4]. Evidence further suggests that this modality performs equally well when imaging radiopharmaceutically dense tumors [5] and that it shows promise in sensitively the axillary lymph nodes [1, 6–8]. With further development scintimammography could prove a valuable complement to traditional screening methods.

For this application, compact scintillator/photodiode cameras offer several advantages over conventional scintillation cameras: (1) arrays of small photodiodes provide improved intrinsic spatial resolution; (2) the small camera size allows shorter imaging distances, thus improving collimator resolution; (3) the compact design permits a greater variety of viewing angles and allows multiple cameras to view different views simultaneously; and (4) the multiple scintillator-photodiode channels yield a higher overall maximum count rate. In this work we characterize a prototype module for a compact camera using optically isolated CsI(Tl) crystals coupled to PIN silicon photodiode arrays. Efforts to develop similar cameras using position sensitive photomultiplier tubes are described in references [9–11].

II. Design Overview

A. Discrete Scintillation Camera Module

The single photon imaging array described in this paper is a prototype for larger modules from which a variety of camera geometries can be realized. A hexagonal hole lead collimator provides directional information, discrete CsI(Tl) crystals convert incident gamma rays to scintillation light, and a photodiode array with custom IC readout circuits these scintillation photons. This design is summarized in Figure 1.

The photodiode arrays were designed for low dark current [12], which is critical to maintaining electronic noise at the long shaping times (~8 μs) that are desirable when using CsI(Tl) crystals. At a bias of 50 V, the 1x3 mm² photodiodes have typical room temperature characteristics of 50 pA dark current, 4 pF capacitance, and 80% quantum efficiency for the 560 nm emissions of CsI(Tl).

A prototype pixel size of 3x3 mm² was chosen as a compromise between several factors. A smaller pixel size both provides slightly better spatial resolution (though this benefit is limited by the fact that the collimator, not pixel size, tends to be the limiting component) and yields lower dark current and capacitance per pixel, which lowers electronic noise. However, using smaller pixels also increases the pixel density and hence the density of electronics required to read out the entire array, which becomes very significant in larger arrays of useful imaging size. Studies on the optimal pixel size for future modules are beyond the scope of this paper.

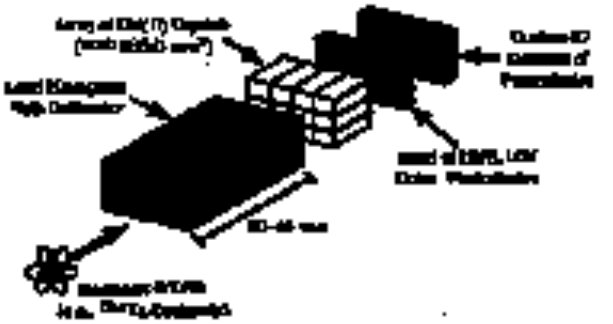

Figure 1: Schematic of a discrete scintillation camera. The prototype has a 2x4 array of pixels, each composed of a 1x3x5 mm³ CsI(Tl) crystal coupled to a 1x3 mm² PIN photodiode. The readout electronics consist of two 3x3 mm² ICs. A camera of similar imaging size can be constructed from an array of individual modules.

[1]This work was supported in part by the U.S. Department of Energy under Contract No. DE-AC03-76SF00098, in part by Public Health Service Grant Nos. P01-HL25840 and R01-CA67911, in part by Breast Cancer Research Program of the University of California Grant No. 1RB-0066, and in part by the Pehr Edman John Heinz Foundation.

B. Custom IC Readout of Photodiodes

The photodiode signals are amplified and shaped by a 16 channel charge sensitive integrated circuit (IC) [13], then processed by a 16 channel "Winner Take All" (WTA) IC [14]. The WTA circuit selects the signal with the largest amplitude, thereby determining both the crystal of interaction (pixel address) and the incident photon energy (signal amplitude). The analog "winner" signal selected by the WTA is sent to a threshold discriminator, and the pulse height is read out with a peak detecting CAMAC ADC. At the same time, the six bit digital address computed by the WTA to identify the "winner" channel is read out with a CAMAC I/O board, and both the digitized signal amplitude and the corresponding address are collected by an acquisition computer. This scheme is shown in Figure 2. A 64 channel IC combining both the charge amplifiers and the WTA circuit has been developed and is currently being tested.

The custom ICs used to read out the photodiode signals are less than 3 mm on a side and can be mounted to the back of the photodiode array, allowing for compact design and facilitating the scaling up from a single module to a full camera composed of an array of such modules. Even a small 5×5 cm^2 imaging array would have about 300 channels, making discrete electronics prohibitively bulky.

C. Collimator Selection

Since the collimator is the limiting factor for both spatial resolution and sensitivity in single photon imaging devices, careful collimator design is critical. Traditional scintillation cameras use hexagonal hole collimators, but in a discrete scintillator camera it is also possible to use square holes matched 1-to-1 (or 4-to-1, etc.) to the square detector pixels. Previous simulations suggest that for square pixel detector arrays, matched square holes provide a superior spatial resolution/sensitivity tradeoff compared to hexagonal holes [15]. Additionally, matching square collimator holes to the detector pixels provides a point spread function with minimal depth-dependence on source position by eliminating the blurring due to geometric mismatch between hexagonal collimator holes and square detector pixels. Hexagonal hole collimators, however, have a more symmetric septal penetration pattern and generally result in shorter collimators for the same sensitivity (because hexagonal holes can usually be made smaller than matched square holes, as the former do not share the latter's convention of matching to the size of the detector pixels).

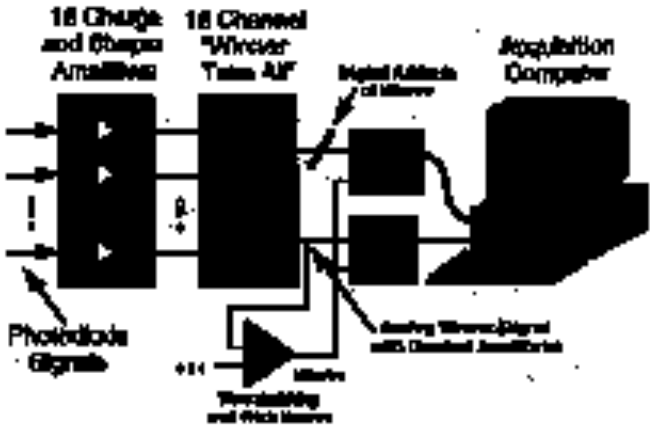

Figure 2. Current IC readout of photodiode array. The first IC amplifies and shapes the photodiode signals, and the WTA IC selects the signal with the greatest amplitude and passes it plus a six bit digital address denoting the "winner" channel on to an acquisition computer. Each IC is 3×3 mm in size.

To first order the spatial resolution of either a hexagonal or square hole collimator is:

$$\text{spatial resolution} = 2 \cdot \frac{w}{h} \cdot \left(d + \frac{h}{2} \right) \qquad (1)$$

where w is the hole size, h the collimator height, and d the imaging distance. This equation thus loosely defines two imaging ranges: the near field, where the collimator geometry term ($h/2$) is dominant, and the far field, where the imaging distance d is dominant. An imaging distance equal to roughly half the collimator height—or about 10–15 mm for many of the compact multipinhole discussed in this paper—is the approximate crossover point between the two.

In the far field, the resolution is limited by the collimator aspect ratio (assuming the intrinsic resolution is sufficiently fine). In the near field, gamma rays from a point source entering over a collimator hole tend to penetrate mostly one hole, so if the collimator is matched to the detector pixel, the spatial resolution is determined by the pixel size and not the collimator aspect ratio. As the collimator sensitivity is approximately proportional to the square of the collimator aspect ratio for both the near and far field, the classical collimator resolution/sensitivity tradeoff does not hold in the near field and fine resolution can be achieved without compromising sensitivity by reducing w and h proportionally. Given discrete square detector pixel elements (and assuming no collimator penetration), this advantage can be fully realized with a matched square hole collimator, but only partially realized with a hexagonal hole collimator (because geometric mismatch can allow two or more detector pixels to be exposed to gamma rays even if only one collimator hole is penetrated).

Potential for improving the resolution/sensitivity tradeoff thus arises when the object is in the near field of the collimator, which corresponds to an imaging distance of less than roughly half the height h of the collimator. Finer resolution in this region can be achieved by reducing the hole diameter w, but maintaining high sensitivity requires a corresponding reduction in h, which then reduces the extent of the near field. The collimator designs that we are currently exploring have a height h of 1.5–6.5 mm, limiting the imaging distance where these gains can be made to a maximum of 0.75–3.25 mm. As we wish to image breast lesions at distances as great as 5 cm, we cannot rely on the near field benefits to provide superior performance across the entire imaging range. Hence we must consider both near and far field performance when selecting a collimator geometry.

Measurements presented in this paper were made using hexagonal hole collimators primarily because of their greater commercial availability. Our Monte Carlo simulations indicate that if the hexagonal collimator holes are small relative to pixel size (approximately: hole diameter $< 0.5 *$ pixel size), the spatial resolution degradation due to the slanting rays between the collimator holes and detector pixels is small. This will be further addressed and quantified in subsections III.D and III.E.

III. Detector Imaging Characteristics

A. Background Spectrum

We observe low count rates for the 3x8 array when there is no radiation source present. The average across all 12 pixels is 0.24 events/pixel/sec above a 50 keV threshold, and 0.018 counts/pixels/sec within the 126–154 keV energy window commonly used for ^{99m}Tc. This rate of background activity is consistent with cosmic ray flux. The summed spectrum for the entire array is shown in Figure 3.

B. Energy Resolution

The 12 pixels in the 3x4 detector array demonstrate an average room temperature energy resolution of 11.7±0.9% fwhm for the 140 keV emissions of ^{99m}Tc at amplifier shaping times of 8 μs (clinical) and 24 μs (full). However, the 53 nm thickness of the anti-reflective (AR) coating for this photodiode array was optimized for 410 nm light and not the 540 nm emissions of CsI(Tl), preventing complete collection of the scintillation photons. Calibration using the direct interaction of 5.9 keV ^{55}Fe gammas in silicon photodiodes (and assuming 3.6 eV per electron-hole pair generation) showed that the average signal amplitude in these measurements was 5400 e-. This value is very similar to the results reported in [10], wherein various cylindrical CsI(Tl) crystals (9 mm diameter, 1–9 mm height) read out with Hamamatsu photodiodes (S3590-3 and S2744-04) demonstrate an average signal level of 5387 e-.

We tested a second 2x4 detector array using an identical CsI(Tl) array coupled to a photodiode array with an AR coating optimized for CsI(Tl) (68 nm thickness, close to 1/4 the wavelength of 540 nm photons in a medium with an index of refraction of 1.9). The average signal amplitude increased to 6600 e-, and the average energy resolution dropped to 10.7±1.6% fwhm. A typical photopeak for this array is shown in Figure 4. The measurements of spatial resolution reported in the remainder of the paper, however, were made on the first detector array.

The choice of 8 μs shaping time (9 μs rise, 24 μs fall) provides the most accurate energy resolution despite the fact that the noise minimum for the amplifier/photodiode electronics occurs near 4 μs. The electronic noise at this shaping time is about 345 e- fwhm, compared to 360 e- fwhm at 8 μs. However, the slow decay component of CsI(Tl) scintillation light (as large as 3 μs decay time) imply that more scintillation photons are collected at 8 μs than at 4 μs, and this increase in signal is larger than the associated

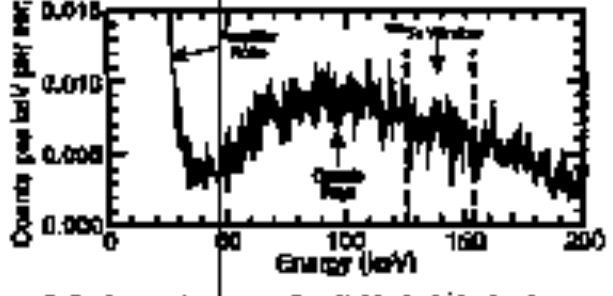

Figure 3. Background spectrum for all 12 pixels in the detector array. There are 0.24 counts/channel/sec above 50 keV, and 0.015 counts/channel/sec in the 126–154 keV ^{99m}Tc window.

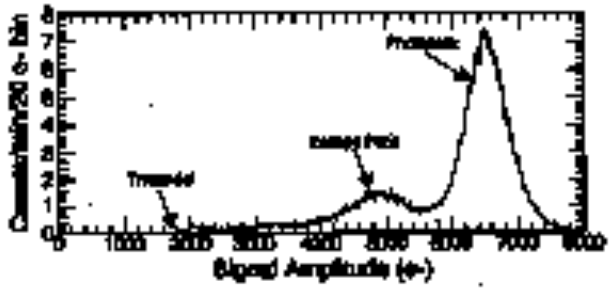

Figure 4. Room temperature ^{99m}Tc photopeak for a typical pixel. Amplifier shaping times were 8 μs rise and 24 μs fall. The signal amplitude is 6530 e- and the photopeak width is 660 e- fwhm, yielding an energy resolution of 10.4% fwhm. The average energy resolution for all array pixels is 10.7±0.9% fwhm.

increase in noise. At a shaping time of 8 μs, the electronic noise is 5.9% fwhm of the 6600 e- signal. The statistical noise is only 2.8% fwhm, leaving an additional 8.5% fwhm contribution (assumed to be due to the inhomogeneity of light collection in the CsI(Tl) crystals) in order to account for the average photopeak width of 10.3% fwhm.

There is potential to further improve the energy resolution and match or surpass the 6–9% fwhm achieved in traditional scintillation cameras. Signal amplitude can be increased by using higher quality CsI(Tl) arrays, as the crystals we used suffer from depth of interaction effects (i.e., scintillation photons absorbed as they traverse the crystal) and suboptimal surface quality (preventing some scintillation photons from reaching the photodiode). Additionally, advances in the charge amplifier IC should reduce the electronic noise, and there remains the possibility of cooling the instrumentation to 5° C to lower dark currents and reduce the associated shot noise. Similar CsI(Tl)/photodiode technology in a cooled environment has demonstrated an energy resolution of 7.5% fwhm for the 122 keV emissions of ^{57}Co [11].

C. Intrinsic Spatial Resolution

When scanning a 2.5 mm diameter collimated ^{57}Co beam across the central row of four crystals in the CsI(Tl) array, we observe an average spatial resolution of 3.3 mm fwhm. Given the significant source diameter, this resolution is consistent with the crystal size of 3 mm and implies that electronic and Compton crosstalk are minimal. The responses of the four individual pixels are displayed in Figure 5.

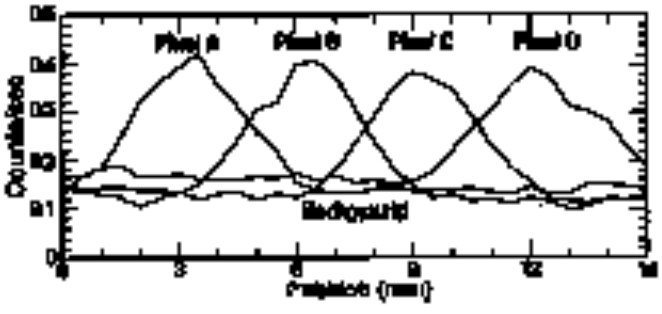

Figure 5. Response of the central row of four pixels to a 2.5 mm diameter ^{57}Co collimated beam scanned across the face of the CsI(Tl) array. The average spatial resolution is 3.3 mm fwhm. Significant background activity is apparent because the source activity was less than 30 uCi.

D. Spatial Resolution: High Resolution Collimator

The spatial resolution of the complete prototype module—including a high resolution collimator—was evaluated in air by scanning a 2 mm diameter collimated ^{99m}Tc source across the middle row of four pixels at imaging distances of 0.0, 2.5, and 5.0 cm (from the front face of the collimator). This is the imaging range of interest for clinical applications because with solid breast compression, most tumors to be imaged will be within 5 cm of the collimator surface. The collimator used has 1.5 mm diameter hexagonal holes and a length of 32 mm, yielding a sensitivity of about 4500 events/mCi/sec. The average spatial resolution of the four pixels is 4.1 mm fwhm at a distance of 0.0 cm, 4.8 mm fwhm at 2.5 cm, and 5.9 mm fwhm at 5.0 cm. Individual pixel responses are displayed in Figure 6.

Monte Carlo simulations of spatial resolution were performed to compare measured results with theoretical predictions, as well as to compare a standard hexagonal hole collimator to a collimator with square holes matched either 1-to-1 or 4-to-1 to the square CsI(Tl) crystals. The simulation determines the average spatial resolution across 25 different point source locations in order to prevent advantageous or disadvantageous positions from dominating the results. An infinitesimally small point source was assumed, septal penetration was not accounted for, and spatial resolutions in the x and y directions were weighted equally. The measured averages and simulated results are presented in Figure 7.

There is some discrepancy between the measured and simulated results for the hexagonal hole collimator. This can be partially accounted for by the fact that the experimental point source was 2 cm in diameter compared to an infinitesimally small simulated one, and by the existence of a ~1 mm air gap between the scintillator array and the collimator in the experimental setup that was not in simulation (this gap was present due to bulky RMI shielding that will be minimized in future modules). However, simulation of these effects indicates that they account for only 0.3 mm of the 0.9 mm spatial resolution difference between experiment and simulation at a 5 cm imaging distance. The remaining difference is likely the result of septal penetration and the penetration of gamma through part of one crystal before being absorbed in another crystal, neither of which were included in simulations.

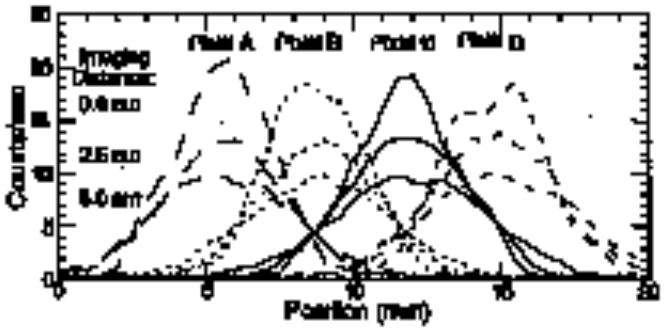

Figure 6. Response of one center row of four pixels behind a high resolution hexagonal hole collimator to a 2.0 mm diameter collimated ^{99m}Tc source scanned across at imaging distances of 0.0, 2.5, and 5.0 cm. The average spatial resolution at these distances is 4.1 mm fwhm, 4.8 mm fwhm, and 5.9 mm fwhm, respectively. Measurements were performed in air. The collimator has a sensitivity of 4300 events/mCi/sec.

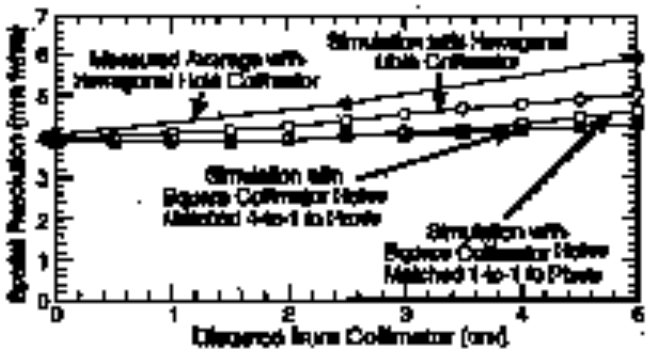

Figure 7. Average spatial resolution versus imaging distance for measured (see Figure 6) and simulated results with high resolution collimators. The simulated hexagonal hole collimator has an identical geometry as the experimental collimator, the 1-to-1 matched square hole collimator is 32 mm long with 2.0x2.0 mm^2 holes (0.2 mm septal thickness) resulting unit cells 3.0x3.0 mm^2), and the 4-to-1 matched square hole collimator is 30 mm long with 1.3x1.3 mm^2 holes (0.2 mm septal thickness) resulting unit cells 1.5x1.5 mm^2). All collimators have sensitivities of about 4500 events/mCi/sec.

The simulation results of Figure 7 suggest that a 1-to-1 matched square hole collimator provides slightly better spatial resolution than a hexagonal one. The average improvement across the 0-5 cm imaging range is 0.32 mm fwhm. This comes at the expense of a collimator that needs to be quite long (66 mm) in order to achieve comparable sensitivity, which is contrary to the goal of compact design. Simulations suggest that using a comparable sensitivity 4-to-1 matched square hole collimator improves the average spatial resolution by an additional 0.08 mm fwhm and requires a collimator length of only 30 mm. A hexagonal hole collimator with the same sensitivity but a more preferable geometry than the one we used (1.0 mm holes instead of 1.5 mm holes) would still be shorter at 30 mm.

In simulations the hexagonal hole collimator exhibits more dependence on source location than do either of the square hole collimators. The spatial resolution of the hexagonal hole collimator over the 25 source locations demonstrates a standard deviation of 0.47 mm (this is the average of the individual standard deviations at different imaging distances in the 0-5 mm range). The standard deviation for both the 1-to-1 and 4-to-1 square hole collimators is 0.45 mm. Despite this very minor difference, there are extreme cases where the spatial resolution of the hexagonal hole collimator is as high as 7.0 mm fwhm (2.1 mm above the average), while for the square hole collimators the worst resolution was 4.9 mm fwhm (0.5 mm above the average).

Our simulations suggest that the missing artifacts that result from slight mismatch between hexagonal collimator holes and square scintillator crystals decrease with decreasing hexagonal hole diameter, and the majority of these missing artifacts become very small once the diameter is less than half the pixel size. Lower limits on the hole diameter are set, however, by manufacturing limitations and by the fact that septal thickness cannot be scaled down along with hole diameter. Collimators with hexagonal holes as small as 1.0 mm are readily available from industry and demonstrate promising spatial resolution and sensitivity characteristics with a discrete detector array when simulated.

E. Spatial Resolution: High Sensitivity Collimator

An extremely important consideration in collimator design is the classic tradeoff between spatial resolution and sensitivity. When imaging in the far field, the sensitivity is roughly proportional to the spatial resolution squared, hence a small degradation in the collimator resolution can yield a significant sensitivity improvement. We repeated the measurements described in subsection III.D using a hexagonal hole collimator with nearly twice the sensitivity of the high resolution collimator. This high sensitivity collimator has 2.6-mm diameter holes, a length of 32 mm, and a sensitivity of 8200 events/mCi/sec. The average observed spatial resolution is 4.3 mm fwhm at a 0.0-cm imaging distance, 5.3 mm fwhm at 2.5 cm, and 6.5 mm fwhm at 5.0 cm. Observed and simulated spatial resolutions for this collimator, as well as simulations for 1-to-1 and 4-to-1 matched square hole collimators of comparable sensitivity, are shown in Figure 8.

When using the high sensitivity hexagonal hole collimator, the measured spatial resolution degrades an average of 0.50 mm fwhm compared to the high resolution collimator. The associated doubling in sensitivity, however, would decrease patient dose, decrease imaging time, and/or improve counting statistics. The high sensitivity hexagonal hole collimator demonstrates a worse spatial resolution in measurements than in simulation for the same reasons discussed in subsection III.D.

The simulated 1-to-1 matched square hole collimator (47 mm long) demonstrates an average spatial resolution improvement of 0.31 mm fwhm compared to the simulated hexagonal hole collimator, while the 4-to-1 square hole collimator (21 mm long) exhibits a further improvement of 0.17 mm fwhm. As with the high resolution collimators, a high sensitivity hexagonal hole collimator with 1.0 mm holes would be shorter yet at 13 mm.

The standard deviation of the spatial resolution demonstrated by the simulated hexagonal hole collimator averaged 0.06 mm, compared to 0.37 mm and 0.38 mm for the 1-to-1 and 4-to-1 square hole collimators, respectively. A few extreme cases are evident, as the maximum spatial resolution of the hexagonal hole collimator is 8.5 mm fwhm (2.8 mm above average), whereas the worst resolution exhibited by either square hole collimator is 5.9 mm fwhm (0.6 mm above average).

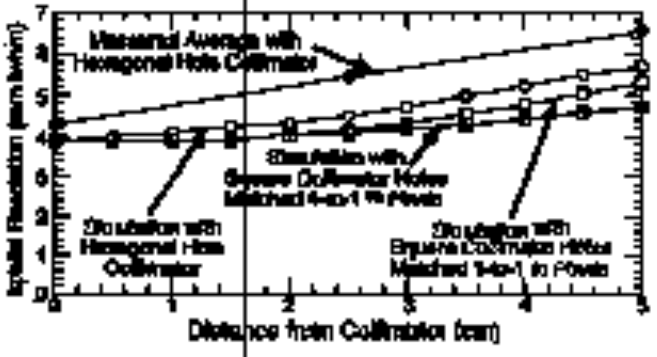

Figure 8. Average spatial resolution versus imaging distance for high sensitivity collimators. The simulated hexagonal hole collimator has an identical geometry to the experimental collimator, the 1-to-1 matched square hole collimator is 47 mm long with 2.6x2.6 mm^2 holes (0.2 mm septal thickness makes unit cells 3.0x3.0 mm^2), and the 4-to-1 matched square hole collimator is 21 mm long with 1.3x1.3 mm^2 holes (0.2 mm septal thickness makes unit cells 1.5x1.5 mm^2). All collimators have sensitivities of about 8200 events/mCi/sec.

IV. Conclusions

Two advances that now make discrete scintillation camera technology a viable option for scintimammography applications are the low leakage current (~50 pA/pixel) photodiode arrays and the custom IC readout of the photodiode signals. Low leakage current is critical to achieving low electronic noise (especially at longer shaping times), which in turn improves the signal-to-noise ratio and hence the energy resolution. Custom IC readout of the photodiode arrays is important to achieving a compact, more effective design, because with the many pixels that will be present in a complete camera, discrete electronics become prohibitively bulky and expensive.

The prototype 3x4 pixel discrete scintillation camera module demonstrates good energy and spatial resolution characteristics that suggest a full camera consisting of an array of modules would prove a successful radionuclide imaging device. An average energy resolution of 10.7% fwhm was demonstrated for ^{99m}Tc, and observations by other researchers indicate that faster CsI(Tl) crystals and matched electronics can yield an energy resolution as low as 7.5% fwhm. There is some hope that this discrete scintillation camera technology can meet or even surpass the 6–9% fwhm energy resolution typically demonstrated by conventional scintillation cameras.

The spatial resolution observed when using a high resolution hexagonal hole collimator (4300 events/mCi/sec) is 3.9 mm fwhm at 5 cm (the anticipated maximum breast-to-camera imaging distance), and simulations suggest the potential to improve to less than 3 mm fwhm. This good spatial resolution is notable because scintimammography with conventional scintillation cameras is poor at detecting tumors less than 1 cm in diameter. The proposed discrete, compact cameras should be able to see significantly smaller lesions.

Collimator design has a crucial impact on camera performance. With hexagonal hole collimators, increasing the sensitivity from 4300 to 8200 events/mCi/sec degrades the spatial resolution by only about 0.5 mm fwhm over the 0–5 cm imaging range, from 4.1–5.9 mm fwhm to 4.3–6.5 mm fwhm. Simulations suggest that the choice of a 1-to-1 matched square hole collimator over a hexagonal one of comparable sensitivity improves spatial resolution by an average of about 0.4 mm fwhm, but at the cost of a longer, less compact collimator. A 4-to-1 matched square hole collimator further improves spatial resolution by about 0.1 mm and allows a reasonably short collimator. The spatial resolution of both square hole collimator configurations demonstrates less dependence on source location than that of a comparable hexagonal hole collimator. The hexagonal collimators should have a more uniform septal penetration pattern, but this effect was not included in the simulations.

The advantages and disadvantages inherent in the choice between hexagonal and matched square hole collimators,

however, will have a much smaller impact on the ability of a camera to detect breast lesions than will the traditional tradeoff between spatial resolution and sensitivity. This optimization is heavily dependent on assumptions regarding lesion sizes, relative tracer uptake ratios, imaging distances, and imaging times, making it beyond the scope of this paper.

V. Acknowledgments

We would like to thank Dr. T. F. Budinger for many valuable discussions concerning this project. This work was supported in part by the Director, Office of Energy Research, Office of Health and Environmental Research, Medical Applications and Biophysical Research Division of the U.S. Department of Energy under contract No. DE-AC03-76SF00098, in part by the National Institutes of Health, National Heart, Lung, and Blood Institute and National Cancer Institute under grant No. HL23340 and No. R01-CA67911, in part by the Breast Cancer Fund of the State of California through the Breast Cancer Research Program of the University of California under grant No. 1RB-0068, and in part by the Public and John Hertz Foundation.

VI. References

[1] R. Taillefer, A. Robidoux, S. Turpin, et al., "Detection of axillary lymph node involvement with Tc-99m sestamibi imaging in patients with primary breast cancer," *J Nucl Med*, vol. 37, pp. 97S, 1996.

[2] I. Khalkhali, I. Villanueva-Meyer, E.L. Edell, et al., "Diagnostic accuracy of Tc-99m Sestamibi breast imaging in breast cancer detection," *J Nucl Med*, vol. 37, pp. 74P, 1996.

[3] S. Piccolo, S. Lanzoria, C. Maltoni, et al., "Technetium-99m-methylene diphosphonate scintimammography to image primary breast cancer," *J Nucl Med*, vol. 36, pp. 718–724, 1995.

[4] H. Palmedo, H.H. Biersack, S. Lanzoria, et al., "Scintimammography with Tc-99m MIBI for breast cancer detection: results of the prospective European multicenter trial," *J Nucl Med*, vol. 38, pp. 20–21P, 1996.

[5] I Khalkhali, I. Villanueva-Meyer, E.L. Edell, et al., "Impact of breast density on the diagnostic accuracy of Tc-99m sestamibi breast imaging in the detection of breast cancer," *J Nucl Med*, vol. 37, pp. 74–75P, 1996.

[6] C.H. Kao, S.J. Wang, and S.H. Yeh, "Tc-99m MIBI uptake in breast carcinoma and axillary lymph node metastases," *Clin Nucl Med*, vol. 19, pp. 898–900, 1994.

[7] H. Palmedo, A. Bohnenberg, F. Grunwald, et al., "Technetium-99m-sestamibi-mammography for suspicious breast lesions," *J Nucl Med*, vol. 37, pp. 626–630, 1996.

[8] W.W.M. Leon, W.T. Yang, Y.L. Chan, et al., "Detection of axillary lymph node metastases in breast carcinomas by technetium-99m sestamibi breast scintigraphy, ultrasound, and conventional mammography," Eur J Nucl Med, vol. 23, pp. 498–503, 1996.

[9] J. Strobel, N.H. Cilsholme, and W.L. Rogers, "Design studies for a cesium iodide silicon photodiode gamma camera," *J Nucl Med*, vol. 38, pp. 3D, 1997.

[10] C.S. Levin, E.J. Hoffman, M.F. Tornai, et al., "Design of a small scintillation camera with photodiode readout for imaging malignant breast tumors," *J Nucl Med*, vol. 37, pp. 32P, 1996.

[11] B.E. Patt, J.E. Iwanczyk, M.F. Tornai, et al., "Dedicated breast imaging system based on a novel solid state detector array," *J Nucl Med*, vol. 38, pp. 142P, 1997.

[12] K.S. Holland, M.W. Wang, and W.W. Moses, "Development of low noise, back-side illuminated silicon photodiode arrays," *IEEE Trans Nucl Sci*, NS-44, pp. 443–447, 1997.

[13] W.W. Moses, I. Kipnis, and M.H. Ho, "A 16-channel charge sensitive amplifier IC for a PIN photodiode array based PET detector module," *IEEE Trans Nucl Sci*, NS-41, pp. 1469–1473, 1994.

[14] W.W. Moses, I. Kipnis, and M.H. Ho, "A 'whatever-you-will' IC for determining the crystal of interaction in PET detectors," *IEEE Trans Nucl Sci*, NS-43, pp. 1615–1618, 1996.

[15] M.F. Tornai, B.E. Patt, J.E. Iwanczyk, C.S. Levin, et al., "Electron scintillator coupled cesium iodide photodetector array for breast imaging," *IEEE Trans Nucl Sci*, NS-44, pp. 1127–33, 1997.

[16] M. Moszynski, M. Kapusta, M. Mayhugh, et al., "Absolute Light Output of Scintillators," *IEEE Trans Nucl Sci*, NS-44, pp. 1021–1061, 1997.